Andean Geology 51 (3): 460-474. September, 2024
doi: 10.5027/andgeoV51n3-3669

Andean Geology
www.andeangeology.cl

Conjugate Riedel shears in a volcanic caldera: the case of the Laguna del Maule Volcanic Complex, Central Chile

***Alvar Pastor Castilla[1], Macarena Constanza Contreras Osses[2], Isaac Corral Calleja[3]**

[1] *Departamento de Obras Civiles y Geología, Universidad Católica de Temuco, Rudecindo Ortega 2950, Temuco 4780000, Araucanía, Chile.*
apastor@uct.cl

[2] *Doctorado en Planificación Territorial y Sustentabilidad, Facultad de Recursos Naturales, Universidad Católica de Temuco, Rudecindo Ortega 2950, Temuco 4780000, Araucanía, Chile.*
m.contrerasosses@gmail.com

[3] *Departament de Geologia, Universitat Autónoma de Barcelona, Carrer dels Til·lers, 08193 Bellaterra, Barcelona, Spain.*
isaac.Corral@uab.cat

**Corresponding author: apastor@uct.cl*

ABSTRACT. The Andean intra-arc is characterized by large-scale continuous lineaments, often the direct surface expression of tectonic structures. In this study, we analyze the main lineaments around the Laguna del Maule Volcanic Complex, Central Chile (~36° S), to shed light on the main tectonic processes. We show that the lineament directions are consistent with structures based on a theoretical Riedel model and suggest the occurrence of two conjugate Riedel shears crossing Laguna del Maule. This structural arrangement can accommodate deformation related to either a transtensional regime, having a WNW-oriented master fault (Laguna Fea Fault), or a transpressional regime, characterized by NNE-oriented master faults (*e.g.*, Melado Fault). In this context, the NE-striking Troncoso Fault would be a long-lived dextral fault compatible with both regimes. According to the Riedel model, ENE-oriented lineaments are predicted to be tensional structures, whilst NW-oriented structures (*e.g.*, Los Cóndores Fault) would correspond to P-type structures accommodating compressional deformation. This tectonic architecture, characterized by the most intense deformation just at the intersection between shears, has likely promoted magma accumulation and would explain the compositional variability at Laguna del Maule. This study therefore demonstrates the usefulness of oriented lineament maps in interpreting regional tectonics for volcanically active areas.

Keywords: Riedel, Volcanic caldera, Geologic lineaments, Southern Volcanic Zone, Laguna del Maule.

RESUMEN. Modelo de deformación Riedel en una caldera volcánica: el caso del Complejo Volcánico Laguna del Maule, Chile Central. El intrarco andino está caracterizado por la presencia de lineamientos continuos de carácter regional, los que frecuentemente son la expresión superficial directa de estructuras tectónicas mayores. En este estudio se presenta un análisis de los principales lineamientos en torno al Complejo Volcánico Laguna del Maule, ubicado en Chile Central (~36° S), para proveer inferencias sobre los principales procesos tectónicos en la zona. Los resultados obtenidos indican que las direcciones de los lineamientos principales pueden ser explicados por un modelo teórico de deformación Riedel. La distribución espacial de ellos sugiere la ocurrencia de dos bandas de cizalla conjugadas, las que dividen la Laguna del Maule. Esta disposición estructural puede acomodar la deformación asociada tanto a un régimen transtensional, caracterizado por una falla maestra orientada ONO (Falla Laguna Fea), como a un régimen transpresional, caracterizado por fallas maestras orientadas al NNE (*e.g.*, Falla Melado). En este contexto, la Falla Troncoso, de orientación NE, sería de tipo dextral transcurrente bajo cualquiera de los dos regímenes. Los lineamientos ENE, en tanto, corresponderían a estructuras tensionales, mientras que los lineamientos NO (*e.g.*, Falla Los Cóndores) serían estructuras tipo P, acomodando la deformación compresional. Este marco tectono-estructural, caracterizado por una deformación más intensa donde las bandas de cizalla se cortan, facilitaría la acumulación de magma en profundidad y explicaría la variación composicional de los productos volcánicos del Complejo Volcánico Laguna del Maule. Este estudio, en consecuencia, demuestra que los mapas de lineamientos orientados pueden ser de gran utilidad para interpretar la tectónica regional en áreas volcánicas activas.

Palabras clave: Riedel, Caldera volcánica, Lineamientos geológicos, Zona Volcánica Sur, Laguna del Maule.

1. Introduction

The study of tectonics in the intra-arc Andean region, particularly in the Southern Volcanic Zone (SVZ; ~33-46° S), presents significant challenges due to the complexity of deformation processes and their associated structures, the abundance of recent volcanic products, and the intense glacial erosion (*e.g.*, Rosenau *et al.*, 2006; Cembrano and Lara, 2009). Crustal deformation due to plate convergence is unevenly accommodated by fault systems in the intra-arc region, resulting in both margin-parallel (N-to-NNE) and margin-oblique (~NW) faults (*e.g.*, Cembrano *et al.*, 2000; Melnick *et al.*, 2006; Rosenau *et al.*, 2006; Pérez-Flores *et al.*, 2016). These structural domains exhibit diverse yet interconnected fault geometries and kinematics (*e.g.*, Sielfeld *et al.*, 2019a).

Riedel shears (Riedel, 1929) are a well-documented phenomena associated with strike-slip faults developed in relatively homogeneous rock lithologies and typically in a cover sequence over a transcurrent basement structure. In the SVZ, the interaction between margin-parallel and ~NW-striking Andean transverse faults results in rhomb-shaped domains, typically related to Riedel-type deformation. This structural array manifests at the surface in kilometer-scale morphostructural lineaments (*e.g.*, Cembrano and Lara, 2009; Piquer *et al.*, 2016; Salas *et al.*, 2016; Giambiagi *et al.*, 2019), which can be measured, quantified, and interpreted (*e.g.*, Rosenau, *et al.*, 2006; Göllner *et al.*, 2021).

Large, regional-scale continuous lineaments are often the direct surface expression of deep structures that can be used to trace down fracture zones (Tripathi *et al.*, 2000; Jordan *et al.*, 2005; Solomon and Ghebreab, 2006; Soto-Pinto *et al.*, 2013; Han *et al.*, 2018). The spatial pattern of these lineaments is typically characteristic of the stress field that causes tectonic deformation. However, the mapping and interpretation of tectonic lineaments are complex tasks and require the inspection and integration of a number of geological and geomorphological features. Remote sensing techniques provide additional information on the spatial arrangement and distribution of faults and fractures in large and geologically variable areas (*e.g.*, Grohmann, 2004; Jordan and Schott, 2005; Hashim *et al.*, 2013; Soto-Pinto *et al.*, 2013; Flores-Prieto *et al.*, 2015). In recent years, extraction methods of geological lineaments from remote sensor data have focused on improving the algorithms for recognizing the linear geospatial components of raster images (*e.g.*, Ahmadi and Pekkan, 2021). Many studies (*e.g.*, Han *et al.*, 2018; Abdelouhed *et al.*, 2021; Villalta Echeverría *et al.*, 2022) employ increasingly complex methods for the automatic extraction of lineaments and present results that seem to fit well with local tectonics, however, there is still no method successfully tested in different geological contexts (Ahmadi and Pekkan, 2021).

Our study therefore focuses on an area centered around the Laguna del Maule Volcanic Complex (Fig. 1A and B), which benefits from recent research providing numerous field measurements and detailed structural characterizations (Garibaldi *et al.*, 2020; Sielfeld *et al.*, 2019b) (Fig. 1C). The primary motivation of this study was to devise a semi-automated lineament extraction method, an aspect deemed relevant due to the challenges in formulating a systematic methodology for the extraction and analysis of lineaments in the intra-arc Andean region. This contribution underscores the importance of lineament analysis as a valuable tool for advancing the understanding of regional tectonic processes, particularly in volcanically active regions.

2. Geological setting

The Laguna del Maule Volcanic Complex (LdMVC) is located at ~36° S, at the divide between Chile and Argentina (Fig. 1A and B). This volcanic field covers ~500 km^2 of the Andean intra-arc zone with Quaternary lavas and tuffs (*e.g.*, Hildreth *et al.*, 2010; Singer *et al.*, 2014). The LdMVC has a few large edifices with at least 130 identified vents, from which >350 km^3 of volcanic products have erupted since around 1.5 Ma (Andersen *et al.*, 2017; Hildreth, 2021). The LdMVC hosts a ~96 km^2 volcanic caldera, whose northern half includes the Laguna del Maule lake, surrounded by 36 postglacial rhyolite and rhyodacite coulees and domes that erupted from 24 separate vents (Hildreth *et al.*, 2010; Singer *et al.*, 2014; Hildreth, 2021). Although there have been no historical eruptions, the extensive Holocene volcanism and significant uplift rates since at least 2007 (*e.g.*, Fournier *et al.*, 2010; Feigl *et al.*, 2014; Le Mével *et al.*, 2015; Singer *et al.*, 2018) make this volcanic field one of the most hazardous volcanic systems in the SVZ (Stern, 2004; Romero *et al.*, 2024). The drainage network around the volcanic caldera takes

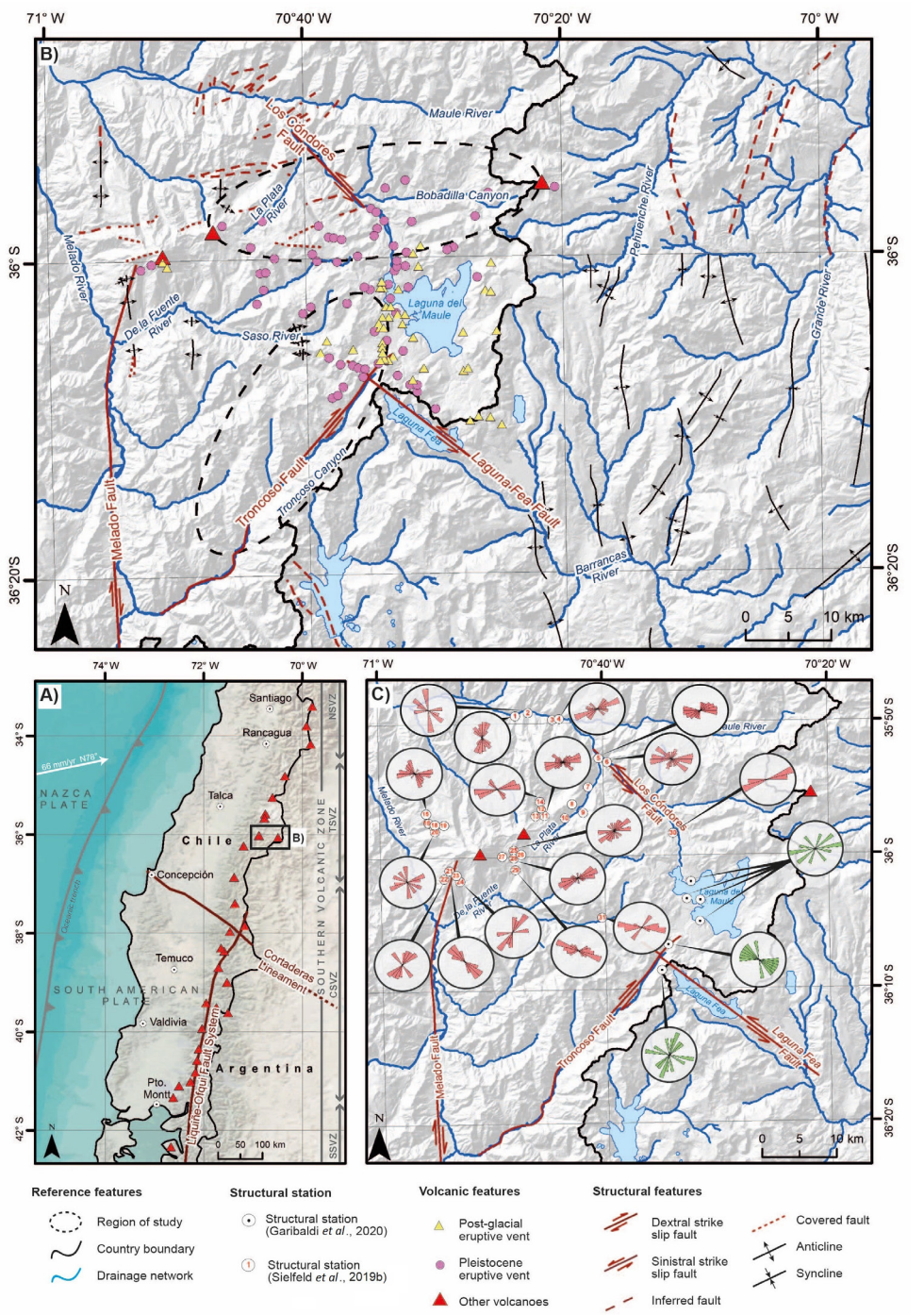

FIG. 1. **A.** Synthesis map of the Southern Volcanic Zone (SVZ) of the Andes and the main regional-scale tectonic structures. Arc segmentation after López-Escobar *et al.* (1995): Northern SVZ (NSVZ; 33-34.5° S), Transitional SVZ (TSVZ; 34.5-37° S), Central SVZ (CSVZ; 37-41.5° S), and Southern SVZ (SSVZ; 41.5-46° S). **B.** Hillshaded relief of the study area, centered around the Laguna del Maule Volcanic Complex, highlighting the drainage network. This map displays the locations of places referred to in the text, as well as the location of all relevant eruptive vents, faults and folds. Dashed ellipsoids delineate the two areas with structural characterizations that were chosen for the application and testing of the lineament extraction method. **C.** Hillshaded relief with the drainage network and structural information from previous studies, represented as rosette plots (data from Sielfeld *et al.*, 2019b and Garibaldi *et al.*, 2020).

on an overall annular shape and is formed by four main rivers that flow outward from it (Fig. 1B). Several segments of the drainage network follow straight valleys, and some of these valleys coincide with the major strike-slip faults identified in the region (Cardona *et al.*, 2018; Sielfeld *et al.*, 2019b).

Recent published tectonic models of the LdMVC describe a NE-oriented transtensional zone that hosts the magmatic system (Miller *et al.*, 2017; Cardona *et al.*, 2018; Peterson *et al.*, 2020). One such example is the Troncoso Fault (Fig. 1B), which corresponds to a NE-striking long-lived fault that reaches the LdMVC from the SW. The Troncoso Fault represents the limit between two different types of deformation and has apparently influenced post-glacial volcanism in the LdMVC area (Cardona *et al.*, 2018; Garibaldi *et al.*, 2020). In fact, the fault's hanging wall (northwestern block) localizes numerous, small-volume rhyodacitic and andesitic volcanic deposits (Andersen *et al.*, 2017), and contains abundant NNE-to-NE striking normal faults (Garibaldi *et al.*, 2020; Peterson *et al.*, 2020) (Fig. 1C). By contrast, the fault's footwall (southeastern block) has few N-S striking faults (Peterson *et al.*, 2020) and ample evidence of rhyolitic eruptions, particularly during the late Holocene (Singer *et al.*, 2014, 2018; Andersen *et al.*, 2017). The arc-oblique, Andean Transverse faults (ATFs), represented by the WNW-striking Laguna Fea Fault and the NW-striking Los Cóndores Fault (Fig. 1B and C), also seem to strongly influence magma emplacement (Cardona *et al.*, 2018; Sielfeld *et al.*, 2019b).

3. Methodology

Our working hypothesis was that the directionality of the drainage network would exhibit similar trends to that of the tectonic structures. To test this hypothesis, we developed a semi-automatic lineament extraction method (Fig. 2). The method relies on the drainage pattern and involves a statistical approach, and it was tested in two data-rich areas (Fig. 1B and C; Sielfeld *et al.*, 2019b; Garibaldi *et al.*, 2020; Peterson *et al.*, 2020). These areas were: 1) an ENE-oriented ellipsoid centered in the Los Cóndores Fault, and 2) a NE-oriented ellipsoid parallel to the Troncoso Canyon.

After successfully testing the lineament extraction method and azimuthal statistics in these two regions,

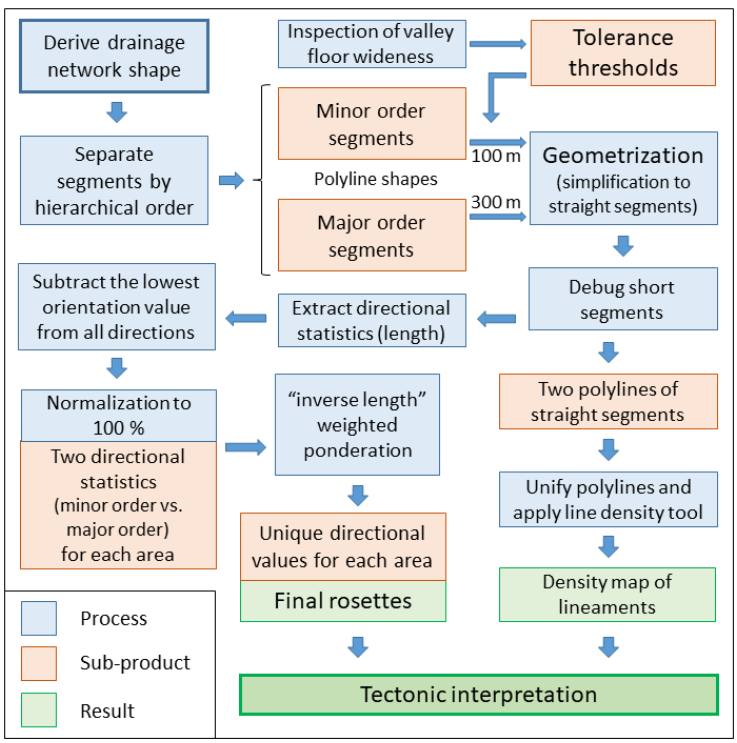

FIG. 2. Flowchart depicting the methodological steps followed in this study.

we then proceeded to apply it to an approximately 4,500 km^2 area, centered around the LdMVC. We identified the predominant tectonic trends and conducted a comprehensive multiscale analysis. In order to facilitate the interpretation of regional tectonic patterns, the outcomes of our analysis are presented in the form of rosette diagrams and density maps of oriented lineaments.

3.1. Derivation of drainage network and Strahler order

In this study, the drainage network was derived from the ALOS PALSAR Digital Elevation Model (spatial resolution of 12.5 m), based on the D8 (multidirectional method) method using the Hydrology Toolset (Tarboton *et al.*, 1991) in ArcGIS. The D8 model algorithm determines the flow direction based on water flow from a given cell into only one adjacent cell. The flow accumulation was calculated from the flow direction raster by assigning a threshold for the minimum contributing area (Jenson and Domingue, 1988), which also determines the drainage densities (*e.g.*, Colombo *et al.*, 2007).

The directional orientation of channels within the drainage network is widely recognized to vary according to their hierarchical order (*e.g.*, Resmi *et al.*, 2019; Duvall *et al.*, 2020; Saidi *et al.*, 2020). The stream order was based on the Strahler classification and also obtained from digital elevation data using specific GIS tools. The azimuthal statistics of the minor (1st and 2nd orders) and the major (3rd to higher) order channels were calculated separately. It is worth to mention that what is considered a first-order channel is relative, since it depends on the contributing area threshold whereby the drainage network is derived (see above). Thus, the minimum contributing area determines the resulting stream ordering. A given basin can have segments of usually 4 to 7 hierarchical orders depending on the size of the basin. The minimum drainage area considered to be representative depends on the spatial resolution of the digital elevation model since it also controls the number, length, and density of lineaments (*e.g.*, Smith and Wise, 2007; Das and Pardeshi, 2018; Meixner *et al.*, 2018; Rajasekhar *et al.*, 2018; Soliman and Han, 2019). In this study, an accumulation threshold of 1,600 cells (0.25 km^2 in total) was used as a routine criterion.

3.2. Segment geometrization process

The drainage network consists of meandering lines, which need to be transformed into straight segments so it can then be converted into linear lineaments. The Douglas-Peucker algorithm facilitates the transformation of the original drainage network into a series of rectilinear segments (Douglas and Peucker, 1973). This process is commonly referred to as 'geometrization' or 'simplification' of polylines. This process dismisses the local sinuosity due to the dynamics of the river itself or external factors, such as the contribution of sediments from valley sides. This algorithm is used to reduce the number of points needed to represent a river segment by assigning an amplitude tolerance threshold, which defines the maximum distance that any point (vertex) of the original river path can be laterally separated from the straight line that best fits the original river segment. Therefore, the tolerance threshold used to simplify the drainage network defines what is accepted as the local sinuosity of a river without disturbing its linear trend. A smaller tolerance distance generates more well-fitted straight segments to the original rivers, whereas a larger tolerance simplifies the drainage network as fewer straight segments are needed to represent it. Thus, the tolerance threshold controls the number of segments and their mean length, which is a fundamental parameter for defining tectonic lineaments (*e.g.*, Han *et al.*, 2018; Saidi *et al.*, 2020). The mean length of segments increases when a wider tolerance is used.

In this study, we posit that variations in channel amplitude and valley width exist among river segments of differing hierarchical orders. Consequently, the tolerance thresholds employed to derive lineaments need to be adjusted according to the ordering of the river segments, specifically their valley floor amplitude. To establish suitable values for these tolerance thresholds, we conducted multiple measurements using Google Earth, basing our criteria on the absolute amplitude of the channels. Our measurements indicate that main rivers are generally straight (with a sinuosity index of less than 1.2), with some local sinuosity caused by endogenic dynamic processes such as dejection cones from the lateral hillslopes, lava flows, or localized meandering sections. On the other hand, minor-order segments are streams embedded in the hillslopes with limited lateral mobility. Therefore, we used a tolerance threshold of 100 meters to simplify

the minor-order segments and 300 meters for major-order segments. An example of this procedure can be seen in figure 3 for the neighboring Tatara-San Pedro complex. After the geometrization process, we eliminated the segments shorter than the width tolerance to avoid the accumulation of small line segments that may have been deviated from their original orientation during geometrization.

3.3. Azimuthal statistics

After segmenting the drainage network based on channel ordering and converting it into straight segments, we harnessed specialized GIS tools to extract statistical data regarding the direction and length of these straight channel segments. Two distinct sets of lineament statistics were obtained, corresponding to minor- and major-order channels respectively. Following this, we identified the azimuth associated with the shortest lineament and subtracted this value from all orientations. We made this adjustment because we regard the azimuth with the shortest length as a representation of 'background noise' or the outcome of random stream orientations unrelated to tectonic activity. Subsequently, we normalized the resulting length values to 100% to obtain length percentages for each direction and calculated the average of the normalized azimuthal statistics for minor and major streams within each analyzed area, regardless of their absolute length. All this process yielded a unified lineament statistics dataset. The newly derived percentages implicitly involved a weighting operation, where the weights assigned to minor- and major-order segments in the final average would be inversely proportional to their absolute lengths. For instance, in our case study the cumulative length of minor-order segments is nearly three times greater than that of higher-order segments. As a result, when we calculate the average of the normalized percentages for each direction, higher-order channels, despite their

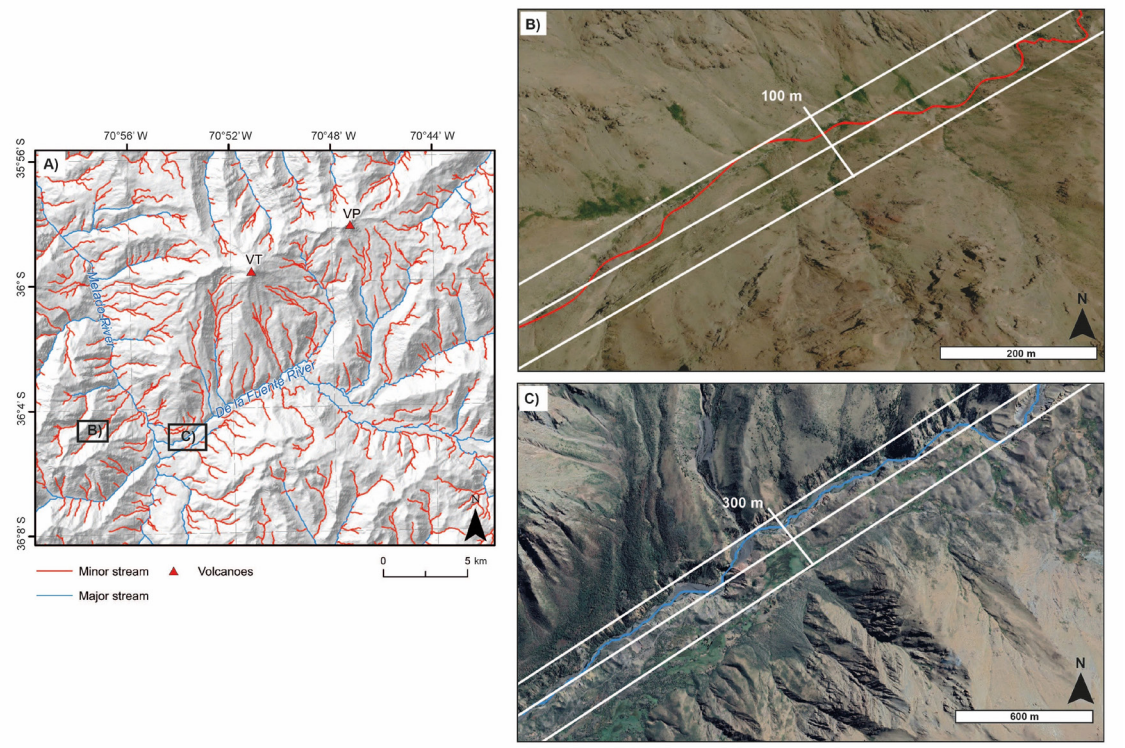

FIG. 3. **A.** Hillshaded map centered around the Tatara San Pedro Volcanic Complex (VT) and the Pellado Volcano (VP), west from Laguna del Maule (see Fig. 1 for locations). Drainage network depicts the main rivers (blue) and minor-order streams (red) according to their hierarchical ordering. **B.** Example of geometrization process for minor-order catchments, applying a tolerance threshold of 100 m. **C.** Example of geometrization process for major-order rivers, with a tolerance threshold of 300 m.

shorter total length, carry a more significant weight in the final azimuth statistics. In consequence, the dominant trends within the higher-order segments exert a considerable influence on the subsequent rosette diagram.

3.4. Density map of straight drainage segments

After obtaining the polylines of straight segments representing the original drainage network, we created length-weighted density maps of lineaments. These density maps highlight the longest straight segments, typically associated with geologic lineaments. The maps were derived from the Line Density algorithm in ArcGIS, by assigning a search radius of 0.5 km and the segment length as a weighting parameter. To better recognize and interpret the tectonic structures, we produced density maps of lineaments in two different azimuths: 0-90° and 90-180°. The tectonic interpretation of lineaments was achieved by integrating the length-weighted density maps of lineaments with the drainage network, in conjunction with the incorporation of structural data from previous studies.

4. Results

The azimuthal statistics of lineaments derived from the drainage network are presented in different rose plots (Fig. 4). The directionality of the drainage network, prior to any statistical treatment, shows very uniform roses, with almost no discernible dominant trends at the regional scale (first column in figure 4). The azimuthal statistics of minor-order segments also creates relatively uniform rose plots, displaying a subtle overall tendency in minor areas (second column in figure 4). On the other hand, major-order segments, which are aligned with the directions of the main valleys, exhibit clear preferential trends (third column in figure 4). Finally, the last plot (fourth column in figure 4) represents the combined azimuthal statistics of minor- and major-order segments, weighted according to their absolute lengths.

The processed azimuthal statistics of lineaments for the Los Cóndores Canyon, present five preferential azimuthal trends: 60-70°, 40-50°, 10-30°, 110-120°, and a spread of NW-NNW directions. The Troncoso

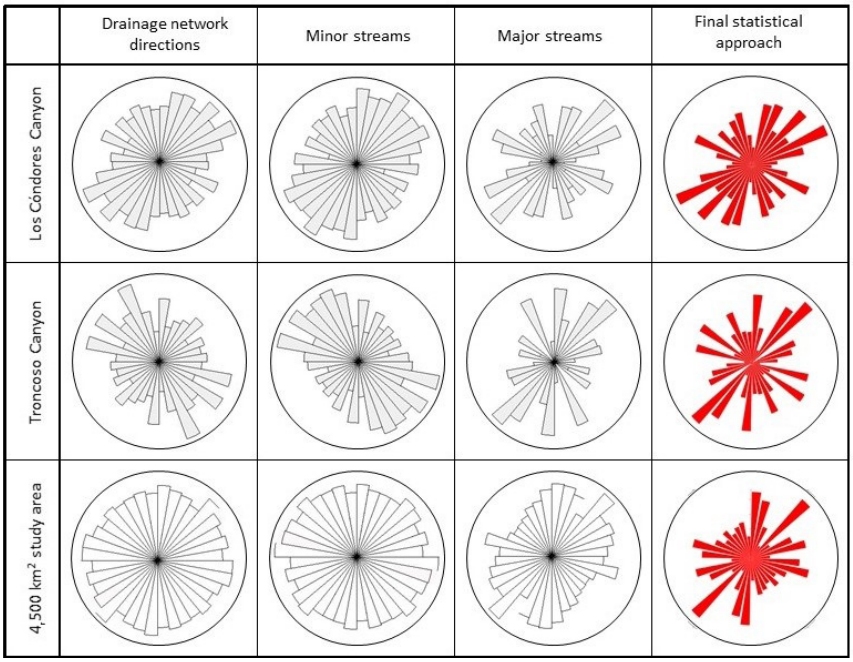

FIG. 4. Rose plots with 10° bins illustrating the orientations of lineaments derived from the drainage network for two designated testing areas (Los Cóndores and Troncoso; see figure 1B) and across the entire region. The first column depicts the trend of the drainage network (considering an accumulation threshold of 0.25 km^2). The second and third columns showcase minor- and major-order channel orientations, respectively. The diagrams in the fourth column represent the length-weighted lineaments following the statistical methodology described in the text.

Canyon also shows five main azimuthal trends: 30-50°, 0-10°, 100-110°, 120-130°, and 150-160°. Finally, the results for the whole 4,500 km^2 study area suggest the main trends 40-50°, 0-20°, 60-80°, 100-120°, and a less clear spread of NW directions.

All drainage-derived lineaments are shown in a density map (Fig. 5A). In order to facilitate the representation of juxtaposed sets of structures, we present two separate density maps of lineaments: 0-90° and 90-180°, respectively, each highlighting a specific set of structures (Fig. 5B and C).

5. Discussion

In this section, we discuss the advantages of the lineament extraction and quantification method used in this study. By integrating the lineament analysis with insights from previous tectonic studies, we also reinterpret the tectonic framework of the 35.5-36.5° S Andean intra-arc region.

5.1. Lineament extraction for multiscale analysis

This study used the drainage pattern shape (instead of other possible lineament sources) for the lineament extraction and subsequent analysis. The relationship between drainage network and tectonics is generally conditioned by the Strahler orders (*e.g.*, Resmi *et al.*, 2019; Saidi *et al.*, 2020). The direction of the higher-order segments is usually related to main tectonic structures, whereas lower-order segments probably reflect other factors, like lithological contrasts (*e.g.*, Gioia *et al.*, 2018; Duvall *et al.*, 2020) or the local relief (*e.g.*, Ribolini and Spagnolo, 2008; Gioia *et al.*, 2018). For this reason, the spatial distribution and frequency of lineaments in a given orientation can vary significantly according to the observation scale (*e.g.*, Barth *et al.*, 2012) and depends on the size of the studied area (*e.g.*, Xu *et al.*, 2020). Within this context, the azimuthal statistics of higher-order segments is probably enough to broadly characterize the major tectonic trends but could not be representative at more local scales. One the other hand, shorter lineaments related to minor-order segments are significant, particularly when conducting azimuthal analysis at the local scale, as relying solely on the main valleys may not adequately represent all relevant tectonic structures. For instance, structures following the NW to WNW direction are not represented by major streams within the Troncoso Canyon (third column in figure 4), but they are by lateral tributaries of lower Strahler orders (second column in figure 4).

The main advantage of deriving lineaments solely from the drainage network is the flexibility to use different tolerance thresholds during the line extraction process, depending on the prior categorization of river segments. The tolerance threshold determines how much a segment of the drainage network can deviate from a straight line to be simplified as such. In simple terms, a higher tolerance threshold allows for the creation of longer lineaments for higher-order segments, while a lower tolerance helps maintain the original direction for lower-order segments. The choice of the tolerance threshold was made here based on a geomorphological criterion, such as the average width of the valleys (Fig. 3B and C). For larger rivers, which typically flow through wider valleys and experience greater lateral channel mobility due to natural processes, we used larger tolerance thresholds. Conversely, for smaller tributaries and hillslope streams, we employed shorter tolerance thresholds to preserve their original directions. This way, both higher- and lower-order segments were considered by assigning different weights for different-order streams in the statistical counting of lineaments. Our statistical approach increased the importance of the larger but scarce lineaments (related to main rivers) with respect to the shorter, but more numerous, lineaments (related to minor-order streams), hence favoring a coherent representation of the structural framework.

5.2. Lineament analysis and its consistency with the Riedel Model

The azimuthal statistics obtained from lineaments in both local and regional domains reveal five main trends, broadly consistent with the angular patterns of a Riedel-type structural system (Figs. 5 and 6). The basic geometry of the Riedel structure (Riedel, 1929) consists of characteristic angular relationships and kinematics associated with the structures that develop over time under a fairly consistently oriented stress regime. The sequential development of shear surfaces in natural Riedel systems is still poorly understood, but there is general consensus in that as the shear zone evolves, the strain within the Riedel system is accommodated by synchronous movement on all fractures comprising the zone.

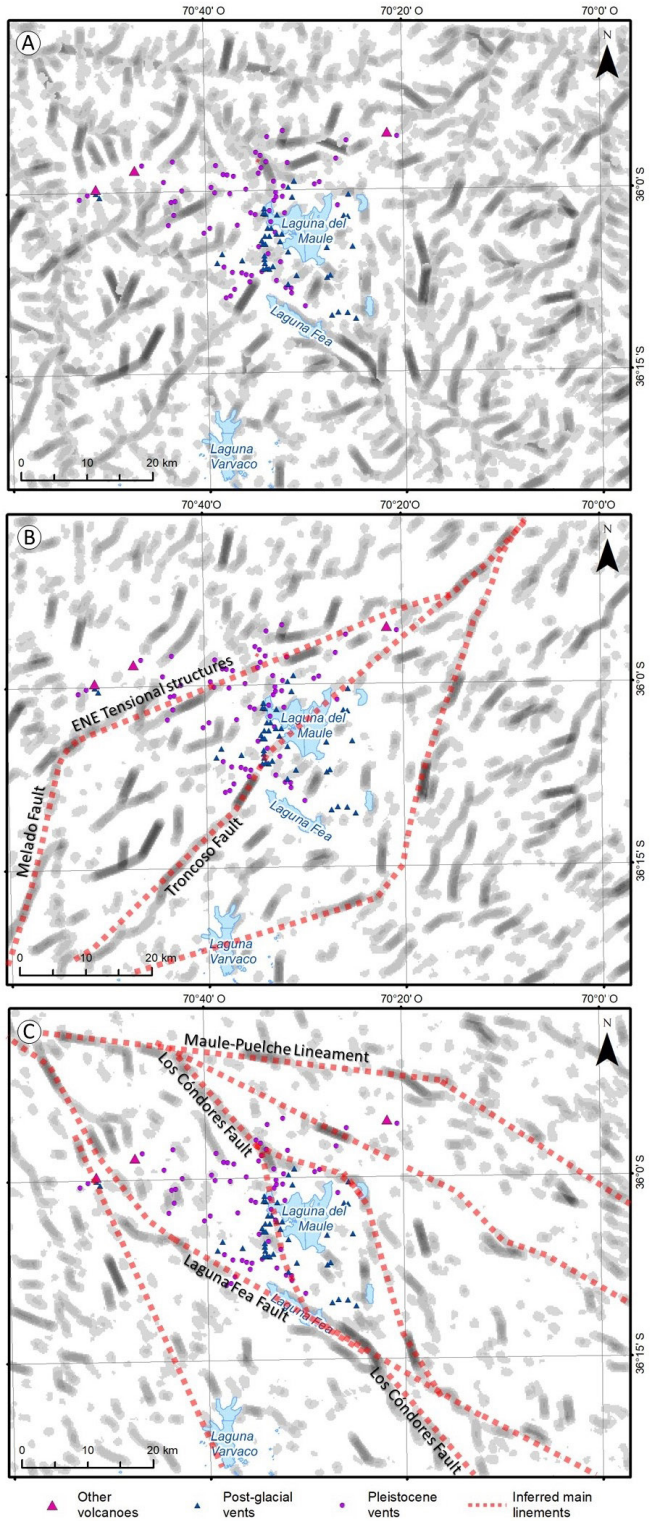

FIG. 5. **A.** Density maps of lineaments. **B.** Density maps of oriented lineaments trending 0-90°. **C.** Density maps of oriented lineaments trending 90-180°. All maps show the characteristic structural features.

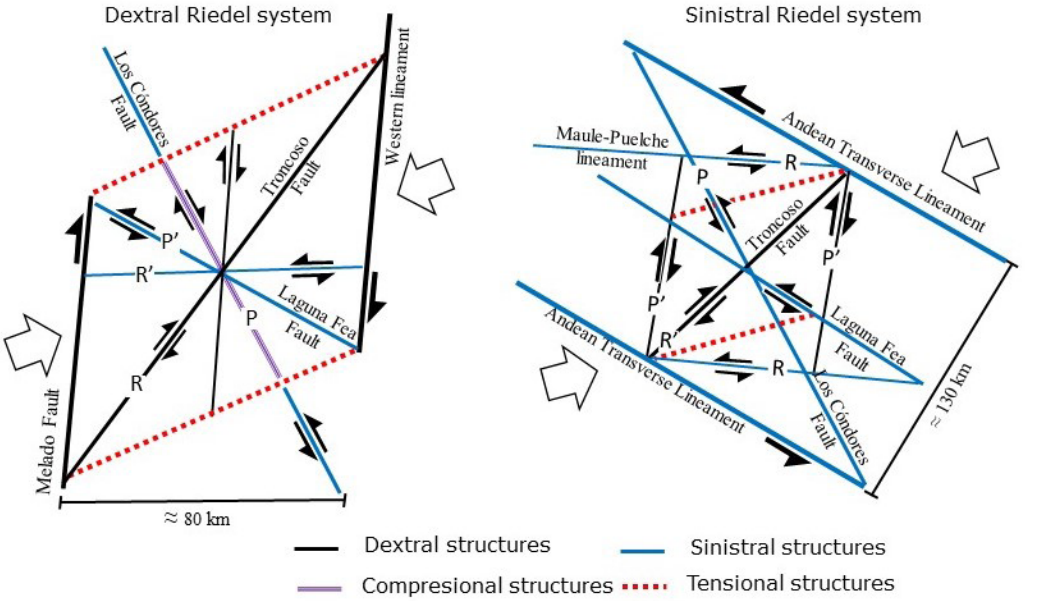

FIG. 6. Schematic representation of two Riedel models: a dextral Riedel system oriented NNE (left diagram) and a sinistral Riedel system oriented WNW (right diagram). The main tectonic structures defined in the study area and their theoretical positions in each of the models are also shown. Additionally, the type of structure (R, P, R' and P', according to the Riedel model) and its presumed sense of motion are specified.

The map depicting the 0-90°-oriented lineaments (Fig. 5B) suggests the occurrence of regional-scale ~N-S and ENE lineaments forming a rhomb-shaped domain of a dextral Riedel system. This feature has the dextral Melado Fault as a western master fault, and the Troncoso Fault as the R-type structure (Fig. 6). Within this framework, the ENE-oriented lineaments are expected to be extensional fractures related to the dextral sense of motion of the NNE-striking master faults, as reported elsewhere in the SVZ (*e.g.*, Lavenu and Cembrano, 1999; Rosenau *et al.*, 2006). Examples of such lineaments in the study area can be recognized along the Tatara Damage Zone, defined as an ENE-oriented transtensional feature bordered by the Troncoso, Laguna Fea, Melado, and Los Cóndores faults (Sielfeld *et al.*, 2019b). The Tatara Damage Zone is characterized by a dense array of faults and fractures and by a generalized presence of ENE-striking normal and strike-slip faults, combined with 60-70° E oriented dyke swarms (Sielfeld *et al.*, 2019b; Ruz *et al.*, 2020). This ENE direction is also consistent with normal faults located in the northern margin of the Laguna del Maule (Bobadilla Canyon; Fig. 1B), previously defined as a series of collapse structures generated after large-magnitude eruptions (Hildreth *et al.*, 2010). According to the lineament analysis, tensional features cross the Los Cóndores Fault and continue further to the east, extending into Argentina (Fig. 5B).

The map showing the 90-180°-oriented lineaments (Fig. 5C) highlights the presence of NW and WNW lineaments, possibly related to the ATFs, broadly documented in the SVZ (*e.g.*, Cembrano and Lara, 2009; Piquer *et al.*, 2019; Pearce *et al.*, 2020). We document clear WNW-trending lineaments crossing the study area, situated immediately north and south of the LdMVC (Fig. 5C). This is consistent with some sinistral NW-to-WNW strike-slip faults reported in the area (*e.g.*, Laguna Fea Fault; Cardona *et al.*, 2018; Garibaldi *et al.*, 2020). We therefore postulate the Laguna Fea Fault as a master fault of a WNW sinistral Riedel system, capable of accommodating local transtensional stresses. In this context, the NW-striking Los Cóndores Fault would represent the P-type structure, characterized by sinistral motion, while the Troncoso Fault would be associated with the R'-type structure, with a dextral sense of motion (Fig. 6).

The ~E-W striking Maule-Puelche lineament stands out as a prominent geological feature that

cut throughout the topography at the northern edge of the study area (Fig. 5C). This trend is coherent with the sinistral R'-type structure within the dextral Riedel system as well as with the sinistral R-type structure within the sinistral Riedel system (Fig. 6). Similarly, the NE-striking lineaments are dextral R type structures within the dextral Riedel system and dextral R'-type structures within the sinistral Riedel system. By contrast, the NW-oriented faults (*e.g.*, Los Cóndores Fault) correspond to P-type structures in both regimes, exhibiting sinistral kinematics in a transtensional regime but dextral kinematics in a transpressional regime (Fig. 6).

5.3. New insights for an updated regional tectonic model

Recent studies proposed that transpression in the SVZ accommodates by distributed deformation (*e.g.*, Sielfeld *et al.*, 2019b; Eisermann *et al.,* 2021). Building upon the interpretation of lineaments and a thorough review of structural characterizations from previous studies, we suggest a coexisting and interacting fault system in the LdMVC area. Specifically, we propose that the NNE-oriented Melado Fault, with dextral motion, and the WNW-oriented Laguna Fea Fault, exhibiting sinistral motion, are the main faults of a Riedel deformation model (Fig. 6).

Some tectonic models of the LdMVC area have suggested a local-scale, NE-oriented pull-apart basin, with the dextral Troncoso Fault as the western master fault (Miller *et al.*, 2017; Cardona *et al.*, 2018; Peterson *et al.*, 2020). In the present study, we rather suggest a larger-scale, rhomb-shaped pull-apart basin (Fig. 5B). This regional structure would have the dextral Melado Fault as a western master fault, and the Troncoso Fault as the cross-basin fault zone, similar to what has been observed in analog models (*e.g.*, Wu *et al.*, 2009). In this framework, the ENE-oriented lineaments correspond to tensional structures, which are coherent with either a transpresional or transtensional regime (Fig. 6).

In the southern SVZ, the tectonic shift from transtensional to transpresional likely took place in the late Pliocene (Göllner *et al.*, 2021). Further north, however, in the LdMVC area, a compressional regime was suggested based on NW- to N-S striking reverse faults affecting recent lacustrine sediments (Garibaldi *et al.*, 2020). The NW-oriented Los Cóndores Fault was previously proposed as a long-lived, arc-oblique ATF, with a sinistral sense of motion (Sielfeld *et al.*, 2019b), although the authors also acknowledged difficulties in determining the fault's kinematics and recognized the presence of dextral NW-oriented structures at the confluence of the Los Cóndores Canyon and the Maule Valley. On the other hand, results from analogue experiments show that regularly spaced NW-striking faults, spontaneously localized as Riedel shears, are inherently related to dextral transpression (Eisermann *et al.*, 2021). Therefore, according to the Riedel model, the Los Cóndores Fault would be a P-type structure capable of shifting its kinematics from sinistral to dextral depending on the prevalent tectonic regime (Fig. 6). The lineament analysis conducted here suggests that this structure branches to accommodate compressional deformation, potentially developing a duplex structure (Fig. 5C). The structure encompasses most of the post-glacial vents in the LdMVC area, suggesting that it could be reactivated in the future.

6. Conclusions

Our analysis, which integrates lineament analysis with insights from previous tectonic studies, suggests that the structural arrangement around the Laguna del Maule area can be modeled by conjugate Riedel shear bands. These shear bands represent regional-scale sets of structures that intersect each other at Laguna del Maule, forming a densely fractured zone. The prevailing transpressional regime in the region, where deformation is primarily accommodated by NNE-oriented faults (*e.g.*, Melado Fault), may locally alternate with transtensional conditions, activating WNW-oriented faults (*e.g.*, Laguna Fea Fault). Within this framework, the occurrence of dextral NE-striking structures (*e.g.*, Troncoso Fault), and the development of tensional ENE-oriented structures, are consistent with both deformational regimes. Conversely, according to the Riedel model, the NW-oriented Los Cóndores Fault would be a P-type structure capable of shifting its kinematics from sinistral to dextral depending on the prevalent tectonic regime. The lineament analysis conducted here suggests that this structure branches in the Laguna del Maule area to accommodate compressional deformation, potentially developing a duplex structure. The ability of conjugate Riedel shear bands in accommodating both transtensional and transpressive deformation could explain the compositional magmatic variability at the LdMVC and influence magmatic residence times.

Acknowledgments

This research was supported by the Dirección de Investigación of the Universidad Católica de Temuco. We extend our gratitude to G. Sielfeld and M.G. Gómez-Vasconcelos for their invaluable assistance in reviewing this manuscript.

The authors declare that they have no known competing financial interests or personal relationships that could have appeared to influence the work reported in this paper.

References

Abdelouhed, F.; Ahmed, A.; Abdellah, A.; Mohammed, I. 2021. Lineament mapping in the Ikniouen area (Eastern Anti-Atlas, Morocco) using Landsat-8 Oli and SRTM data. Remote Sensing Applications: Society and Environment 23: 100606. https://doi.org/10.1016/j.rsase.2021.100606

Ahmadi, H.; Pekkan, E. 2021. Fault-based geological lineaments extraction using remote sensing and GIS- A review. Geosciences 11 (5): 183. https://doi.org/10.3390/geosciences11050183

Andersen, N.L.; Singer, B.S.; Jicha, B.R.; Beard, B.L.; Johnson, C.M.; Licciardi, J.M. 2017. Pleistocene to Holocene growth of a large upper crustal rhyolitic magma reservoir beneath the active Laguna del Maule Volcanic Field, Central Chile. Journal of Petrology 58: 85-114. doi: https://doi.org/10.1093/petrology/egx006

Barth, N.C.; Toy, V.G.; Langridge, R.M.; Norris, R.J. 2012. Scale dependence of oblique plate-boundary partitioning: New insights from LiDAR, central Alpine fault, New Zealand. Lithosphere 4 (5): 435-448. doi: https://doi.org/10.1130/L201.1

Cardona, C.; Tassara, A.; Gil-Cruz, F.; Lara, L.; Morales, S.; Kohler, P.; Franco, L. 2018. Crustal seismicity associated to rapid surface uplift at Laguna del Maule Volcanic Complex, Southern Volcanic Zone of the Andes. Journal of Volcanology and Geothermal Research 353: 83-94. https://doi.org/10.1016/j.jvolgeores.2018.01.009

Cembrano, J.; Lara, L. 2009. The link between volcanism and tectonics in the southern volcanic zone of the Chilean Andes: A review. Tectonophysics 471: 96-113. https://doi.org/10.1016/j.tecto.2009.02.038

Cembrano, J.; Schermer, E.; Lavenu, A.; Sanhueza, A. 2000. Contrasting nature of deformation along an intra-arc shear zone, the Liquiñe-Ofqui fault zone, southern Chilean Andes. Tectonophysics 319: 129-149. https://doi.org/10.1016/S0040-1951(99)00321-2

Colombo, R.; Vogt, J.V.; Soille, P.; Paracchini, M.L.; de Jager, A. 2007. Deriving river networks and catchments at the European scale from medium resolution digital elevation data. Catena 70 (3): 296-305. https://doi.org/10.1016/j.catena.2006.10.001

Das, S.; Pardeshi, S.D. 2018. Comparative analysis of lineaments extracted from Cartosat, SRTM and ASTER DEM: a study based on four watersheds in Konkan region, India. Spatial Information Research 26: 47-57. https://doi.org/10.1007/s41324-017-0155-x

Douglas, D.H.; Peucker, T.K. 1973. Algorithms for the reduction of the number of points required to represent a digitized line or its caricature. Cartographica 10 (2): 112-122. https://doi.org/10.3138/FM57-6770-U75U-7727

Duvall, A.R.; Harbert, S.A.; Upton, P.; Tucker, G.E.; Flowers, R.M.; Collett, C. 2020. River patterns reveal two stages of landscape evolution at an oblique convergent margin, Marlborough Fault System, New Zealand. Earth Surface Dynamics 8: 177-194. https://doi.org/10.5194/esurf-8-177-2020

Eisermann, J.O.; Göllner, P.L.; Riller, U. 2021. Orogen-scale transpression accounts for GPS velocities and kinematic partitioning in the Southern Andes. Communications Earth and Environment 2: 167. https://doi.org/10.1038/s43247-021-00241-4

Feigl, K.L.; Le Mével, H.; Tabrez Ali, S.; Córdova, L.; Andersen, N.L.; DeMets, C.; Singer, B.S. 2014. Rapid uplift in Laguna del Maule volcanic field of the Andean Southern Volcanic zone (Chile) 2007-2012. Geophysical Journal International 196 (2): 885-901. https://doi.org/10.1093/gji/ggt438

Flores-Prieto, E.; Quénéhervé, G.; Bachofer, F.; Shahzad, F.; Maerker, M. 2015. Morphotectonic interpretation of the Makuyuni catchment in Northern Tanzania using DEM and SAR data. Geomorphology 248: 427-439. https://doi.org/10.1016/j.geomorph.2015.07.049

Fournier, T.J.; Pritchard, M.E.; Riddick, S.N. 2010. Duration, magnitude, and frequency of subaerial volcano deformation events: New results from Latin America using InSAR and a global synthesis. Geochemistry, Geophysics, Geosystems 11 (1): Q01003. https://doi.org/10.1029/2009GC002558

Garibaldi, N.; Tikoff, B.; Peterson, D.; Davis, J.R.; Keranen, K. 2020. Statistical separation of tectonic and inflation-driven components of deformation on silicic reservoirs, Laguna del Maule volcanic field, Chile. Journal of Volcanology and Geothermal Research, 389: 106744. https://doi.org/10.1016/j.jvolgeores.2019.106744

Giambiagi, L.; Álvarez, P.; Spagnotto, S.; Godoy, E.; Lossada, A.; Mescua, J.; Barrionuevo, M.; Suriano, J. 2019. Geomechanical model for a seismically

active geothermal field: Insights from the Tinguiririca volcanic-hydrothermal system. Geoscience Frontiers 10: 2117-2133. https://doi.org/10.1016/j.gsf.2019.02.006

Gioia, D.; Schiattarella, M.; Giano, S.I. 2018. Right-angle pattern of minor fluvial networks from the Ionian terraced belt, southern Italy: Passive structural control or foreland bending? Geosciences 8 (9): 331. https://doi.org/10.3390/geosciences8090331

Ghosh, S.; Sivasankar, T.; Anand, G. 2021. Performance evaluation of multi-parametric synthetic aperture radar data for geological lineament extraction. International Journal of Remote Sensing 42 (7): 2574-2593. https://doi.org/10.1007/s00531-021-02068-y

Göllner, P.L.; Eisermann, J.O.; Balbis, C.; Petrinovic, I.A.; Riller, U. 2021. Kinematic partitioning in the Southern Andes (39°S-46°S) inferred from lineament analysis and reassessment of exhumation rates. International Journal of Earth Sciences 110 (7): 2385-2398.

Grohmann, C.H. 2004. Morphometric analysis in geographic information systems: applications of free software GRASS and R. Computers & Geosciences 30 (9-10): 1055-1067. https://doi.org/10.1016/j.cageo.2004.08.002

Han, L.; Liu, Z.; Ning, Y.; Zhao, Z. 2018. Extraction and analysis of geological lineaments combining a DEM and remote sensing images from the northern Baoji loess area. Advances in Space Research 62 (9): 2480-2493. https://doi.org/10.1016/j.asr.2018.07.030

Hashim, M.; Ahmad, S.; Johari, M.A.M.; Pour, A.B. 2013. Automatic lineament extraction in a heavily vegetated region using Landsat Enhanced Thematic Mapper (ETM+) imagery. Advances in Space Research 51 (5): 874-890. https://doi.org/10.1016/j.asr.2012.10.004

Hildreth, W. 2021. Comparative rhyolite systems: Inferences from vent patterns and eruptive episodicities: Eastern California and Laguna del Maule. Journal of Geophysical Research: Solid Earth 126 (7): e2020JB020879. https://doi.org/10.1029/2020JB020879

Hildreth, W.; Godoy, E.; Fierstein, J.; Singer, B. 2010. Laguna del Maule volcanic field: Eruptive History of a Quaternary basalt-to-rhyolite distributed volcanic field on the Andean rangecrest in central Chile. Servicio Nacional de Geología y Minería, Boletín 63: 145 p. Santiago.

Jenson, S.K.; Domingue, J.O. 1988. Extracting topographic structure from digital elevation data for geographic information system analysis. Photogrammetric Engineering and Remote Sensing 54 (11): 1593-1600. https://www.asprs.org/wp-content/uploads/pers/1988journal/nov/1988_nov_1593-1600.pdf

Jordan, G.; Schott, B. 2005. Application of wavelet analysis to the study of spatial pattern of morphotectonic lineaments in digital terrain models. A case study. Remote Sensing of Environment 94 (1): 31-38. https://doi.org/10.1016/j.rse.2004.08.013

Jordan, G.; Meijninger, B.M.L.; Van Hinsbergen, D.J.J.; Meulenkamp, J.E.; Van Dijk, P.M. 2005. Extraction of morphotectonic features from DEMs: Development and applications for study areas in Hungary and NW Greece. International Journal of Applied Earth Observation and Geoinformation 7: 163-182. https://doi.org/10.1016/j.jag.2005.03.003

Lavenu, A.; Cembrano, J. 1999. Compressional-and transpressional-stress pattern for Pliocene and Quaternary brittle deformation in fore arc and intra-arc zones (Andes of Central and Southern Chile). Journal of Structural Geology 21 (12): 1669-1691. https://doi.org/10.1016/S0191-8141(99)00111-X

Le Mével, H.; Feigl, K.L.; Córdova, L.; DeMets, C.; Lundgren, P. 2015. Evolution of unrest at Laguna del Maule volcanic field (Chile) from InSAR and GPS measurements, 2003 to 2014. Geophysical Research Letters 42 (16): 6590-6598. https://doi.org/10.1002/2015GL064665

López-Escobar, L.; Cembrano, J.; Moreno, H. 1995. Geochemistry and tectonics of the Chilean Southern Andes basaltic Quaternary volcanism (37-46°S). Revista Geológica de Chile 22 (2): 219-234. http://www.andeangeology.cl/index.php/revista1/article/view/V22n2-a06

Meixner, J.; Grimmer, J.C.; Becker, A.; Schill, E.; Kohl, T. 2018. Comparison of different digital elevation models and satellite imagery for lineament analysis: Implications for identification and spatial arrangement of fault zones in crystalline basement rocks of the southern Black Forest (Germany). Journal of Structural Geology 108: 256-268. https://doi.org/10.1016/j.jsg.2017.11.006

Melnick, D.; Folguera, A.; Ramos, V.A. 2006. Structural control on arc volcanism: The Caviahue-Copahue complex, Central to Patagonian Andes transition (38°S). Journal of South American Earth Sciences 22 (1-2): 66-88. https://doi.org/10.1016/j.jsames.2006.08.008

Miller, C.A.; Le Mével, H.; Currenti, G.; Williams-Jones, G.; Tikoff, B. 2017. Microgravity changes at the Laguna del Maule volcanic field: Magma-induced stress changes facilitate mass addition. Journal of Geophysical Research: Solid Earth 122 (4): 3179-3196. https://doi.org/10.1002/2017JB014048

Pearce, R.K.; Sánchez de la Muela, A.; Moorkamp, M.; Hammond, J.O.S.; Mitchell, T.M.; Cembrano, J.; Araya

Vargas, J.; Meredith, P.G.; Iturrieta, P.; Pérez-Estay, N.; Marshall, N.R.; Smith, J.; Yáñez, G.; Ashley Griffith, W.; Marquardt, C.; Stanton-Yonge, A.; Núñez, R. 2020. Reactivation of fault systems by compartmentalized hydrothermal fluids in the Southern Andes revealed by magnetotelluric and seismic data. Tectonics 39 (12): e2019TC005997. https://doi.org/10.1029/2019TC005997

Pérez-Flores, P.; Cembrano, J.; Sánchez-Alfaro, P.; Veloso, E.; Arancibia, G.; Roquer, T. 2016. Tectonics, magmatism and paleo-fluid distribution in a strike-slip setting: Insights from the northern termination of the Liquiñe-Ofqui fault System, Chile. Tectonophysics 680: 192-210. https://doi.org/10.1016/j.tecto.2016.05.016

Peterson, D.E.; Garibaldi, N.; Keranen, K.; Tikoff, B.; Miller, C.; Lara, L.E.; Tassara, A.; Thurber, C.; Lanza, F. 2020. Active normal faulting, diking, and doming above the rapidly inflating Laguna del Maule Volcanic Field, Chile, imaged with CHIRP, magnetic, and focal mechanism data. Journal of Geophysical Ressearch: Solid Earth 125 (8): e2019JB019329. https://doi.org/10.1029/2019JB019329

Piquer, J.; Berry, R.F.; Scott, R.J.; Cooke, D.R. 2016. Arc-oblique fault systems: their role in the Cenozoic structural evolution and metallogenesis of the Andes of central Chile. Journal of Structural Geology 89: 101-117. https://doi.org/10.1016/j.jsg.2016.05.008

Piquer, J.; Yáñez, G.; Rivera, O.; Cooke, D. R. 2019. Long-lived crustal damage zones associated with fault intersections in the high Andes of Central Chile. Andean Geology 46 (2): 223-239. http://dx.doi.org/10.5027/andgeoV46n2-3106

Rajasekhar, M.; Raju, G.S.; Raju, R.S.; Ramachandra, M.; Kumar, B.P. 2018. Data on comparative studies of lineaments extraction from ASTER DEM, SRTM, and Cartosat for Jilledubanderu River basin, Anantapur district, A.P, India by using remote sensing and GIS. Data in Brief, 20: 1676-1682. https://doi.org/10.1016/j.dib.2018.09.023

Resmi, M.R.; Babeesh, C.; Achyuthan, H. 2019. Quantitative analysis of the drainage and morphometric characteristics of the Palar River basin, Southern Peninsular India; using bAd calculator (bearing azimuth and drainage) and GIS. Geology, Ecology, and Landscapes 3 (4): 295-307. https://doi.org/10.1080/24749508.2018.1563750

Ribolini, A.; Spagnolo, M. 2008. Drainage network geometry versus tectonics in the Argentera Massif (French-Italian Alps). Geomorphology 93 (3-4): 253-266. https://doi.org/10.1016/j.geomorph.2007.02.016

Riedel, W. 1929. Zur mechanik geologischer brucherscheinungen ein beitrag zum problem der fiederspatten. Zentralblatt für Mineralogie, Geologie und Palaontologie Abteilung B: 354-368.

Romero, J.E.; Vergara-Pinto, F.; Forte, P.; Ovalle, J.; Sánchez, F. 2024, The Andean Southern Volcanic Zone: a review on the legacy of the latest volcanic eruptions. Andean Geology 51 (2): 379-412. http://dx.doi.org/10.5027/andgeoV51n2-3681

Rosenau, M.; Melnick, D.; Echtler, H. 2006. Kinematic constraints on intra-arc shear and strain partitioning in the southern Andes between 38°S and 42°S latitude. Tectonics 25 (4): TC4013. https://doi.org/10.1029/2005TC001943

Ruz, J.; Browning, J.; Cembrano, J.; Iturrieta, P.; Gerbault, M.; Sielfeld, G. 2020. Field observations and numerical models of a Pleistocene-Holocene feeder dyke swarm associated with a fissure complex to the east of the Tatara-San Pedro-Pellado complex, Southern Volcanic Zone, Chile. Journal of Volcanology and Geothermal Research 404: 107033. https://doi.org/10.1016/j.jvolgeores.2020.107033

Saidi, A.; Bouramtane, T.; Achab, M.; Kassou, N.; Kacimi, I.; Tahiri, A.; Valles, V. 2020. The Hough transform algorithm coupled with spatial filtering for the study of geological structuring control on the drainage network: application to the North Oulmes region, Morocco. Arabian Journal of Geosciences 13: 1026. https://doi.org/10.1007/s12517-020-06052-9

Salas, P. A.; Rabbia, O.M.; Hernández, L.B.; Ruprecht, P. 2017. Mafic monogenetic vents at the Descabezado Grande volcanic field (35.5 S-70.8 W): the northernmost evidence of regional primitive volcanism in the Southern Volcanic Zone of Chile. International Journal of Earth Sciences 106: 1107-1121.

Salas, P.A.; Rabbia, O.M.; Hernández, L.B.; Ruprecht, P. 2017. Mafic monogenetic vents at the Descabezado Grande volcanic field (35.5°S-70.8°W): the northernmost evidence of regional primitive volcanism in the Southern Volcanic Zone of Chile. International Journal of Earth Sciences 106: 1107-1121. https://doi.org/10.1007/s00531-016-1357-5

Sielfeld, G.; Lange, D.; Cembrano, J. 2019a. Intra-arc crustal seismicity: Seismotectonic implications for the Southern Andes Volcanic Zone, Chile. Tectonics 38 (2): 552-578. https://doi.org/10.1029/2018TC004985

Sielfeld, G.; Ruz, J.; Brogi, A.; Cembrano, J.; Stanton-Yonge, A.; Pérez-Flores, P.; Iturrieta, P. 2019b. Oblique-slip tectonics in an active volcanic chain: A case study

from the Southern Andes. Tectonophysics 770: 228221. https://doi.org/10.1016/j.tecto.2019.228221

Singer, B.S.; Andersen, N.L.; Le Mével, H.; Feigl, K.L.; DeMets, C.; Tikoff, B.; Thurber, C.H.; Jicha, B.R.; Cardona, C.; Córdova, L.; Gil, F.; Unsworth, M.J.; Williams-Jones, G.; Miller, C.; Fierstein, J.; Hildreth, W.; Vázquez, J. 2014. Dynamics of a large, restless, rhyolitic magma system at Laguna del Maule, southern Andes, Chile. GSA Today 24 (12): 4-10. https://doi.org/10.1130/GSATG216A.1

Singer, B.S.; Le Mével, H.; Licciardi, J.M.; Córdova, L.; Tikoff, B.; Garibaldi, N.; Andersen, N.L.; Diefenbach, A.K.; Feigl, K.L. 2018. Geomorphic expression of rapid Holocene silicic magma reservoir growth beneath Laguna del Maule, Chile. Science Advances 4 (6): eaat1513. https://doi.org/10.1126/sciadv.aat1513

Smith, M.J.; Wise, S.M. 2007. Problems of bias in mapping linear landforms from satellite imagery. International Journal of Applied Earth Observation and Geoinformation 9 (1): 65-78. https://doi.org/10.1016/j.jag.2006.07.002

Soliman, A.; Han, L. 2019. Effects of vertical accuracy of digital elevation model (DEM) data on automatic lineaments extraction from shaded DEM. Advances in Space Research 64 (3): 603-622. https://doi.org/10.1016/j.asr.2019.05.009

Solomon, S.; Ghebreab, W. 2006. Lineament characterization and their tectonic significance using Landsat TM data and field studies in the central highlands of Eritrea. Journal of African Earth Sciences 46 (4): 371-378. https://doi.org/10.1016/j.jafrearsci.2006.06.007

Soto-Pinto, C.; Arellano-Baeza, A.; Sánchez, G. 2013. A new code for automatic detection and analysis of the lineament patterns for geophysical and geological purposes (ADALGEO). Computers & Geosciences, 57: 93-103. https://doi.org/10.1016/j.cageo.2013.03.019

Stern, C. R. 2004. Active Andean volcanism: its geologic and tectonic setting. Revista Geológica de Chile 31 (2): 161-206. http://dx.doi.org/10.4067/S0716-02082004000200001

Tarboton, D.G.; Bras, R.L.; Rodríguez-Iturbe, I. 1991. On the extraction of channel networks from digital elevation data. Hydrological Processes 5 (1): 81-100. https://doi.org/10.1002/hyp.3360050107

Tripathi, N.K.; Gokhale, K.V.G.K.; Siddiqui, M.U. 2000. Directional morphological image transforms for lineament extraction from remotely sensed images. International Journal of Remote Sensing 21 (17): 3281-3292. https://doi.org/10.1080/014311600750019895

Villalta Echeverria, M.D.P.; Viña Ortega, A.G.; Larreta, E.; Romero Crespo, P.; Mulas, M. 2022. Lineament extraction from digital terrain derivate model: A case study in the Girón-Santa isabel basin, South Ecuador. Remote Sensing 14 (21): 5400. https://doi.org/10.3390/rs14215400

Wu, J.E.; McClay, K.; Whitehouse, P.; Dooley, T. 2009. 4D analogue modelling of transtensional pull-apart basins. Marine and Petroleum Geology 26 (8): 1608-1623. https://doi.org/10.1016/j.marpetgeo.2008.06.007

Xu, J.; Wen, X.; Zhang, H.; Luo, D.; Li, J.; Xu, L.; Yu, M. 2020. Automatic extraction of lineaments based on wavelet edge detection and aided tracking by hillshade. Advances in Space Research 65 (1): 506-517. https://doi.org/10.1016/j.asr.2019.09.045

Manuscript received: April 29, 2023; revised/accepted: July 03, 2024; available online: July 09, 2024.